Steady-State and Dynamic Modeling for New Product Design for the Solid-State Polymerization of Poly(Ethylene Terephthalate)

Bruce Lucas,[†] Kevin C. Seavey,[†] and Y. A. Liu*[,†,‡]

SINOPEC/FPCC/AspenTech Center of Excellence in Process Systems Engineering, Department of Chemical Engineering, Virginia Polytechnic Institute and State University, Blacksburg, Virginia 24061, and Office of the President, China Petroleum and Chemical Corporation (SINOPEC), No. 6A, Huixin Street, Chaoyang District, Beijing 100029, China

We model an entire poly(ethylene terephthalate) (PET) solid-state polymerization (SSP) process with precrystallizers, crystallizers, SSP reactors, and dryers using a unified cell approach. This approach builds complex unit-operation models using individual cells, or continuous-stirred-tank reactor (CSTR) models. Each cell considers the essential physical properties, phase equilibrium, polymerization kinetics, mass transfer through the polymer and into the carrier gas, and crystallization kinetics. Our model development involves fundamental chemical engineering principles and advanced software tools, such as Polymers Plus and Aspen Custom Modeler. We analyze both reaction and diffusion in each cell, considering two options: (1) to model diffusion using a second-order partial differential equation (PDE) or a simplified two-film theory and (2) to include or ignore crystallization kinetics. Performing best is the model with a PDE for diffusion and with equations describing crystallization and its effect on reaction and diffusion. We validate the model using commercial plant data of intrinsic viscosity, degree of crystallinity, and acetaldehyde concentration. We are unable to find a suitable set of parameters for other simpler models to represent accurately the plant data in its entirety. After validating our SSP model, we apply it to study the sensitivity of our SSP process on temperature and pellet geometry. For pellets with cross-sectional dimensions of 3.2 mm × 3.2 mm, we vary the length from 1.5 to 3.5 mm and predict the intrinsic viscosity. The model suggests only a mild dependence of intrinsic viscosity on the pellet length. In contrast, our model suggests that, for an increase in temperature of 12 °C, intrinsic viscosity rises by almost 0.1 dL/g. Last, we use our validated model to predict the process changes required to produce a high-viscosity product (1 dL/g). Our model suggests that, with appropriate increases in both reactor temperature and residence time, we can make this product.

1. Introduction

Modern computer-aided design (CAD) in chemical engineering combines mathematics, science, and engineering fundamentals to help us analyze, design, control, and optimize chemical manufacturing processes. In the past, we have applied CAD to develop models of polyolefin and nylon-6 polymerization processes.[1−3] In this work, we develop a model of the crystallization and solid-state polymerization (SSP) processes for poly(ethylene terephthalate) (PET). Specifically, we develop a compartmental model (i.e., cell or continuous-stirred-tank reactor model) which, when linked with other identical compartments, is capable of describing precrystallizers, crystallizers, and SSP reactors.

In each cell, we model both diffusion and reaction. Regarding diffusion, we use a convective boundary condition for the interfacial concentration. Several researchers[4−12] assume a value of zero for this boundary condition. A convection boundary condition allows the interfacial concentration to correctly vary with the gas flow rate, thus affecting the attainable molecular weight. Previous research[13−18] shows that the carrier gas flow rate influences the attainable molecular weight.

Regarding reactions, we use temperature-dependent equilibrium constants. The unit operations in this process operate close to the glass-transition temperature, relative to the melting temperature. The temperature dependence is necessary to properly model these low-temperature operations.

We do not presently include a fundamental enthalpy balance for step-growth polymerization systems and the respective unit operations. In other words, we fix the temperature profile in each unit operation as an input.

The remaining sections of this paper are as follows. Section 2 describes the solid-state PET process in this work. Section 3 summarizes the available process data. Section 4 details model development, including engineering fundamentals and relevant equations. Section 5 presents simulation results. Section 6 demonstrates a model application by predicting the operating conditions required to produce a new grade with the process. Last, Section 7 summarizes our conclusions.

2. Process Description

Solid-state polymerization (SSP) is used to build up the intrinsic viscosity required by certain applications such as soft drink bottle and tire cord. Balint et al.,[19] Brent and Shelley,[20] and Cohn[21] describe typical SSP processes for polyesters. Figure 1 shows our process for the SSP of PET.

All unit operations run between the polymer's T_g (glass-transition temperature, 69 °C) and T_m (melting-point temperature, 265 °C).[22] The PET prepolymer first goes through a pair of precrystallizers. The polymer streams leaving the two precrystallizers both feed into a single crystallizer. Nitrogen from the SSP reactor goes into the crystallizer as well. The crystallized polymer drops in at the top of the reactor and travels downward. Nitrogen flows up through the reactor. The polymer product goes into a nitrogen dryer/cooler and then an air dryer/cooler. The dried and cooled polymer is now ready for packaging. The

* To whom correspondence should be addressed. Tel.: (540) 231-7800. Fax: (540) 231-5022. E-mail: design@vt.edu.
[†] Virginia Polytechnic Institute and State University.
[‡] China Petroleum and Chemical Corporation (SINOPEC).

10.1021/ie0601955 CCC: $37.00
Published on Web 12/07/2006

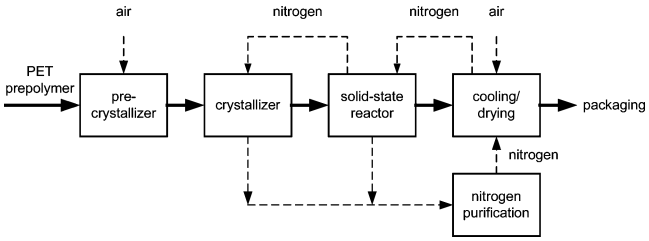

Figure 1. Simplified diagram of our process for SSP of PET.

purified nitrogen contains <30 ppm ethylene glycol, <6 ppm water, and <100 ppm oxygen.

3. Plant Data

3.1. Specification of Polymer Product Grades. We examine three different production grades. The plant produces these grades at different residence times, controlled through chip bed height. All other operating conditions, including the prepolymer feed rate, are the same for each grade. There are two other grades, which we refer to as "design grades" because they have not been produced previously. Table 1 lists the grades.

3.2. Components. Terephthalic acid (TPA) and ethylene glycol (EG) are the monomers. We use the prefixe "t" to denote terminal or end groups, and prefix "b" to represent bound or repeat groups. TPA reacts to give the TPA end group (tTPA) and the TPA bound segment (bTPA). Similarly, EG gives the EG end group (tEG) and the EG bound segment (bEG). Water (W) is a condensation byproduct. Side reactions produce diethylene glycol (DEG) and acetaldehyde (AA). DEG, like the monomers, forms the DEG end group (tDEG) and the DEG bound segment (bDEG). AA can lead to the oxyvinyl end group (tVIN).

We follow the component list given in the literature.[10,23,24] While these references sum up DEG, tDEG, and bDEG together as bDEG, we acknowledge that others elaborate on the DEG formation reactions in their review of PET polymerization kinetics, which includes tDEG and free DEG.[25]

There are two carrier gases in the process: one is primarily nitrogen and the other is air. Air flows through both precrystallizers. Nitrogen is the chosen carrier gas in the crystallizer and reactor. One of the dryers also utilizes nitrogen, while the other utilizes air. Air can theoretically be used as the carrier gas in the reactor, but the oxygen in air may lead to the formation of volatile, low-molecular-weight degradation products that can cause yellowing.[26]

3.3. Unit-Operation Data. There are two precrystallizers operating in parallel. The polymer pellets drop down from the top of the precrystallizer. The polymer chips move horizontally through the box, while hot air blows through the bed. Figure 2 illustrates a single precrystallizer, along with our representation of it in our model.

The polymer from the two precrystallizers feeds into the top of a single crystallizer, which is essentially a vertical column. The polymer pellets are distributed throughout the crystallizer with the aid of cones. Nitrogen flows upward through the falling pellets. We use a series of continuous-stirred-tank reactors (CSTRs) to model the crystallizer.

The SSP reactor is similar in geometry to the crystallizer. The bulk of the SSP occurs here, and the residence time of the reactor determines the final intrinsic viscosity of the product. We also use a series of CSTRs to model the SSP reactor.

After the SSP reactor, the chips enter a cooler. We model the air cooler identically to the way we model the precrystallizer (refer to Figure 2).

Table 2 gives the shape and dimensions of each unit operation that we have discussed.

Table 3 gives scaled operating data for our unit operations, and Table 4 specifies the temperature profile for the SSP reactor.

3.4. Pellet Data. To validate the model, we need to know the average geometry, composition in terms of concentration, degree of crystallinity (x^c), and intrinsic viscosity [η] of the pellets at each stage in the process and for each grade: (1) prepolymer feed (before the precrystallizers); (2) after the precrystallizers; (3) after the crystallizer; and (4) after the solid-state reactor. We can use the mass fraction (x^c) or volume fraction (ϕ^c) of the crystalline phase as our measure of crystallinity. We refer to this fraction as the degree of crystallinity. Many believe that end groups and conventional species exist only in the amorphous phase.[28] Consequently, polymerization only occurs in the amorphous phase.[4] Thermodynamic properties for semicrystalline polymers often use x^c, while crystallization kinetics often use ϕ^c. Our plant measures x^c.

We can convert between x^c and ϕ^c via the following relationship,

$$\phi^c = \frac{x^c/\rho^c}{x^c/\rho^c + (1 - x^c)/\rho^a} \tag{1}$$

where ρ^c and ρ^a are the densities of crystalline and amorphous polymer, respectively. The initial degree of crystallinity is 25% by volume.

Table 5 summarizes our degree of crystallinity and intrinsic viscosity.

The actual pellet shape is cuboid. The average dimensions are 2.5 mm × 3.2 mm × 3.2 mm. The dimensions of the pellet do not change appreciably during the course of processing. We assume a spherical geometry for prepolymer pellets, with a diameter D_p of 2.93 mm.

Our prepolymer pellet has 1.5 wt % W, 11 ppm AA, and trace amounts of TPA, EG, and DEG. The segment fractions for tEG, tTPA, tDEG, tVIN, bEG, bTPA, and bDEG are 0.00731, 0.00241, 0, 0, 0.48402, 0.49514, and 0.01112, respectively. The molar flow rate of polymer molecules is 0.201 kmol/h, and the total molar flow rate of segments is 20.7 kmol/h. There is no catalyst, such as Sb_2O_3, added in this process.

The intrinsic viscosity [η] of a PET resin dictates its grade. The plant measures [η] but not the number-average molecular weight M_n. However, M_n is correlated with intrinsic viscosity. We calculate intrinsic viscosity from the number-average molecular weight in Section 4.2. The intrinsic viscosity of the starting prepolymer is 0.65 dL/g.

4. Model Development

Section 4.1 covers phase equilibrium and physical properties. We correlate the number-average molecular weight and intrinsic viscosity in Section 4.2 and discuss crystallization kinetics in Section 4.3. We present the diffusivities of the volatile components in polymer with initial parameters from the literature in Section 4.4 and establish the SSP kinetics in Section 4.5. Section 4.6 presents the material balance, initial and boundary conditions, and mass-transfer coefficients.

4.1. Phase Equilibrium and Physical Properties. Bokis et al.[29] discuss when to use an activity-coefficient model (ACM) or an equation of state (EOS) for phase-equilibrium calculations. Our system is at low pressure and contains polar species, so we choose an ACM. Chen[32] combines the well-known non-random two-liquid (NRTL)[30,31] ACM model with the Flory–Huggins[33,34] model to represent polymeric species. The result

Table 1. Solid-State PET Grade Recipes

grade	intrinsic viscosity (dL/g)	number-average molecular weight (g/mol)	reactor residence time (h)	application	designation
1	0.81	26 500	10	water bottle	production grade
2	0.85	28 500	12	soft drink bottle	production grade
3	0.87	30 000	16	tray	production grade
4	0.90	31 000	18	plate	design grade
5	≥1.0	≥37 000	>20	tire cord	design grade

Table 2. Geometry of Unit Operations (Dimensions Are Scaled to Protect Intellectual Property)

process unit	general shape	scaled width/diameter	scaled height	scaled length
precrystallizers	cuboid	0.16	0.01	0.33
crystallizer	cylinder	0.26	0.28	
SSP reactor	cylinder	0.22	1.00	
	cone	0.22	0.23	
cooler (nitrogen)	cone	0.23	0.15	
cooler (air)	cuboid	0.15	0.02	0.32

Table 3. Operating Conditions of Vessels

description	scaled temperature	scaled gauge pressure	residence time (h)
precrystallizers	0.12−0.69	0.17	0.67
crystallizer	0.69−0.83	0.43	5
solid-state reactor	0.83−1.00	1.00	10−16
nitrogen cooler	1.00−0.74	1.00	2−3
air cooler	0.74−0.30	0.17	0.5

is the Polymer−NRTL model,[32] which would work well for our process. We find the necessary binary interaction parameters from the following: (1) regression of experimental data published in the open literature (e.g., Yamada et al.[35] have solubility data for the pair EG−TPA); (2) regression of $T-P-x-y$ data in the Dortmund Data Bank, of which AspenTech and DECHEMA also distribute versions; and (3) parameter-estimation techniques that consider the structures of the species. Seavey et al.[36] give guidelines for regressing binary interaction

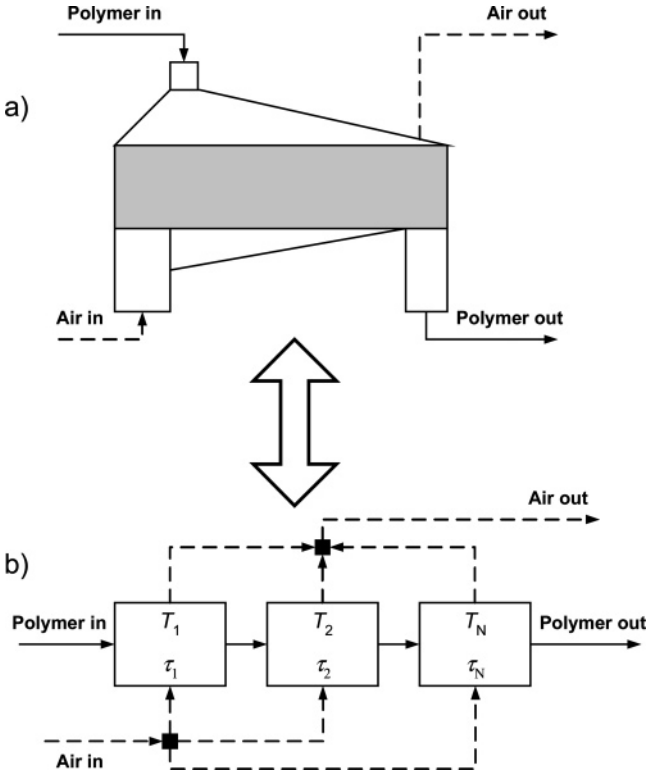

Figure 2. (a) Physical representation of the precrystallizer and (b) our corresponding model. In the figure, T_i and τ_i are the temperature and residence time of stage i, respectively

Table 4. Temperature Profile for the Solid-State Reactor

scaled height	temperature indicator	scaled temperature
0.92	T1	0.95
	T7	0.94
0.75	T2	0.95
	T8	0.95
0.58	T3	0.98
	T9	0.98
0.42	T4	1.00
	T10	1.00
0.25	T5	1.00
	T11	0.99
0.08	T6	0.98
	T12	0.98

parameters for the Polymer−NRTL for nylon-6 polymerization and using them in simulations of two commercial nylon-6 production trains.

We obtain molecular weight and critical properties (temperature, pressure, and molar volume) for conventional species from a property database of the Design Institute for Physical Property Research (DIPPR).[37] We use the correlations and parameters from DIPPR for liquid density ($\hat{\rho}_i^{\mathrm{L}}$), vapor pressure ($P_i^{\mathrm{sat}}$), and vapor viscosity ($\mu_i^{\mathrm{V}}$) of the conventional components.

The density of solid PET pellets varies with the degree of crystallinity. Amorphous PET has a density of 1.33 g/cm^3, while 100% crystalline PET has a density of 1.46 g/cm^3.[21] We calculate the mass density of solid PET using the following equation.

$$\rho_{\mathrm{PET}}^{\mathrm{L}} = x^{\mathrm{c}}\rho^{\mathrm{c}} + (1-x^{\mathrm{c}})\rho^{\mathrm{a}} = x^{\mathrm{c}}\left(1.46\,\frac{\mathrm{g}}{\mathrm{cm}^3}\right) + (1-x^{\mathrm{c}})\left(1.33\,\frac{\mathrm{g}}{\mathrm{cm}^3}\right) \quad (2)$$

The segment mole fraction (F_i) is the fraction of the particular segment in the polymer sample. This is the ratio of the concentration of the segment to the total concentration of all segments.

$$F_i = \frac{C_i}{\sum C_i} \quad (3)$$

The number-average degree of polymerization ($\mathrm{DP_n}$) is the average number of structural units (repeat and end segments) per polymer chain in a polymer sample. We calculate this from the sum of the concentrations of all units divided by the sum of the concentrations of the end groups:

$$\mathrm{DP_n} = \frac{C_{\mathrm{tEG}} + C_{\mathrm{tTPA}} + C_{\mathrm{bEG}} + C_{\mathrm{bTPA}} + C_{\mathrm{bDEG}} + C_{\mathrm{tVIN}}}{C_{\mathrm{tEG}} + C_{\mathrm{tTPA}} + C_{\mathrm{tVIN}}} \quad (4)$$

Note that we have not divided the number of end groups in the denominator by 2 to account for the fact that each polymer molecule has two end groups. This is because the convention for a degree of polymerization for PET is actually two segments, defined as B-EG:B-TPA.

Table 5. Data for Degree of Crystallinity and Intrinsic Viscosity Throughout the Process and for Each Production Grade (The Equivalent Number-Average Molecular Weight Is Given)

				solid-stater exit		
parameter	prepolymer feed	precrystallizer exit	crystallizer exit	(10 h)	(12 h)	(16 h)
x^c (kg/kg)	0.27	0.34	0.40	0.45	0.48	0.51
$[\eta]$ (dL/g)	0.65	0.67	0.70	0.81	0.85	0.87
M_n (kg/kmol)	19 000	20 000	21 000	26 000	29 000	30 000

We calculate the average segment molecular weight of the polymer sample (M_{seg}) by summing the molecular weight of each species (M_i) times F_i.

$$M_{seg} = 2\sum(M_i F_i) \tag{5}$$

Note that M_{seg} approximately equals the molecular weight of a B-EG:B-TPA segment. We can then calculate the number-average molecular weight M_n by

$$M_n = DP_n M_{seg} \tag{6}$$

4.2. Intrinsic Viscosity. We classify the simulation targets into two categories: primary and secondary. The primary targets (intrinsic viscosity, acetaldehyde concentration, and degree of crystallinity) are most important to the daily operation of the plant. The secondary targets (water and ethylene glycol concentrations) serve to help validate the accuracy of the model. We try to match all targets with a minimum error percentage.

Intrinsic viscosity $[\eta]$ dictates the grade of PET. We use the number-average molecular weight (M_n) to calculate $[\eta]$. We start with the Mark−Houwink−Sakurada equation[39]

$$[\eta] = KM_v^a \tag{7}$$

where M_v is the viscosity-average molecular weight and K and a are parameters. Flory[40] gives the ratio assuming a most probable distribution (polydispersity index of 2),

$$M_n/M_v/M_w = 1:[(1+a)\Gamma(1+a)]^{1/a}:2 \tag{8}$$

where M_n is the number-average molecular weight and M_w is the weight-average molecular weight. Therefore, we can write

$$[\eta] = K[(1+a)\Gamma(1+a)]M_n^a \tag{9}$$

$\Gamma(x)$ is the gamma function. The values of K and a for PET are in the *Polymer Handbook*,[41] where the values are dependent on the test method and whether the polymer samples are fractionated or unfractionated. We test intrinsic viscosity with unfractionated samples in phenol/tetrachlorethane (3:2) solvent at 25 °C. Therefore, we use $K = 7.44 \times 10^{-4}$ and $a = 0.648$ from Berkowitz[42] listed in the *Polymer Handbook*. We arrive at the following equation when substituting the values of K and a into eq 9.

$$[\eta] = (11.03 \times 10^{-4})M_n^{0.648} \tag{10}$$

Solid-state PET (or high-intrinsic-viscosity PET) generally has $M_n > 24\,000$, while PET for textile fiber applications (low-intrinsic-viscosity PET) generally has M_n between 17 000 and 21 000.[17] We see that the correlation gives reasonable values for M_n in Table 6.

4.3. Crystallization Kinetics. Table 7 summarizes the crystallization and polymerization kinetics, physical properties, and diffusion models used in this study together with their parameter values.

Table 6. Number-Average Molecular Weight Using the Intrinsic Viscosity Correlation, Equation 11, and Plant Data

sample point	$[\eta]$ (dL/g)	M_n (kg/kmol)
prepolymer feed	0.65	19 000
after the precrystallizers	0.67	20 000
after the crystallizer	0.70	21 000
after the reactor	0.85	29 000

PET undergoes both primary and secondary crystallization.[43] The Avrami equation[44−46] is the most-used equation for describing the kinetics of polymer crystallization. Malkin et al.[47] and Mallon and Ray[48] point out that the Avrami equation only works well during the initial stage of crystallization (primary) for PET but cannot adequately describe secondary crystallization.

We use an equation developed by Malkin et al.[49] to model the crystallization kinetics of PET. This model incorporates heterogeneous nucleation and crystal growth via formation of two-dimensional surface nuclei. Malkin et al.[49] give parameter values for PET in Table 7. One shortcoming of this equation is that it does not account for the effect of moisture on crystallization rate.

The kinetic equation developed by Malkin et al. requires the equilibrium degree of crystallinity, $\phi^{c,0}$. This is the ultimate degree achievable at a given temperature. Although we cannot find data explicitly specifying $\phi^{c,0}$, we are able to find limiting density data (ρ_{lim})[50] that imply $\phi^{c,0}$. The latter is really a function of both temperature and molecular weight. The plant data show ϕ^c increasing with molecular weight. We fit a simple polynomial for $\phi^{c,0}$ as a function of M_n when M_n climbs above a critical point.

4.4. Diffusivity in Polymer. We do not apply the diffusivity equation based on the free volume used by Devotta and Mashelkar[14] to model the diffusivity of the volatile components. Free volume is relevant close to T_g, but industrial reactors always operate >100 °C above T_g, close to T_m. Therefore, we use an Arrhenius expression, which is applicable for all operating temperatures throughout the process. We modify this expression to relate it to the degree of crystallinity. We assume that the crystalline phase excludes the volatile components. We multiply the temperature-dependent diffusivity by a term including the amorphous fraction. Chang[51] and Yoon et al.[7] show that the diffusivity of EG is linearly proportional to the amorphous fraction. Table 7 gives our equation for diffusivity.

Whitehead[52] models the crystallization and drying of PET using an Arrhenius expression for the diffusivity. Mallon and Ray[48] use an Arrhenius expression when modeling a reactor and fit the same activation energy for W and EG. Schmalz and Grundke[53] model the diffusivity of W with an Arrhenius expression. We use the same initial parameters for W and AA. We use parameters from Mallon and Ray for EG and parameters from Schmalz and Grundke for W and AA, which we list in Table 7.

4.5. Polymerization Kinetics. We assume that the reactions in the SSP process are similar to those in the melt state. The types of reaction include the following: (1) esterification; (2) polycondensation; (3) diethylene glycol formation; (4) thermal degradation; (5) acetaldehyde formation; and (6) and vinyl end

Table 7. Polymerization Kinetics, Physical Property, and Diffusion Models Employed in This Study[10,48]

reaction	reaction rate
Esterification	
$EG + TPA \underset{k_1'=k_1/K_1}{\overset{k_1}{\rightleftharpoons}} tEG{:}tTPA + W$	$R_1 = (1-x^c)\left[4k_1\frac{C_{EG}C_{TPA}}{(1-x^c)^2} - \left(\frac{k_1}{K_1}\right)\frac{C_W C_{tTPA}}{(1-x^c)^2}\frac{C_{tEG}}{C_{tEG}+C_{bEG}}\right]$
$EG + tTPA \underset{k_2'=k_2/K_2}{\overset{k_2}{\rightleftharpoons}} tEG{:}bTPA + W$	$R_2 = (1-x^c)\left[2k_2\frac{C_{EG}C_{tTPA}}{(1-x^c)^2} - 2\left(\frac{k_2}{K_2}\right)\frac{C_W C_{bTPA}}{(1-x^c)}\frac{C_{tEG}}{C_{tEG}+C_{bEG}}\right]$
$tEG + TPA \underset{k_3'=k_3/K_3}{\overset{k_3}{\rightleftharpoons}} bEG{:}tTPA + W$	$R_3 = (1-x^c)\left[2k_3\frac{C_{tEG}C_{TPA}}{(1-x^c)^2} - \left(\frac{k_3}{K_3}\right)\frac{C_W C_{tTPA}}{(1-x^c)^2}\frac{C_{bEG}}{C_{tEG}+C_{bEG}}\right]$
$tEG + tTPA \underset{k_4'=k_4/K_4}{\overset{k_4}{\rightleftharpoons}} bEG{:}bTPA + W$	$R_4 = (1-x^c)\left[k_4\frac{C_{tEG}C_{tTPA}}{(1-x^c)^2} - 2\left(\frac{k_4}{K_4}\right)\frac{C_W C_{bTPA}}{(1-x^c)}\frac{C_{bEG}}{C_{tEG}+C_{bEG}}\right]$
Polycondensation	
$tEG + tEG \underset{k_5'=k_5/K_5}{\overset{k_5}{\rightleftharpoons}} bEG + EG$	$R_4 = (1-x^c)\left[k_4\frac{C_{tEG}C_{tTPA}}{(1-x^c)^2} - 2\left(\frac{k_4}{K_4}\right)\frac{C_W C_{bTPA}}{(1-x^c)}\frac{C_{bEG}}{C_{tEG}+C_{bEG}}\right]$
Diethylene Glycol Formation	
$tEG + tEG \xrightarrow{k_6} bDEG + W$	$R_6 = (1-x^c)\left[k_6\frac{C_{tEG}C_{tEG}}{(1-x^c)^2}\right]$
Thermal Degradation	
$bEG{:}bTPA \xrightarrow{k_7} tVIN + tTPA$	$R_7 = (1-x^c)\left[k_7 C_{bEG}\frac{C_{bTPA}}{C_{tEG}+C_{bEG}}\right]$
Acetaldehyde Formation	
$tEG{:}btTPA \xrightarrow{k_8} AA + tTPA$	$R_8 = (1-x^c)\left[k_8\frac{C_{tEG}}{(1-x^c)}\frac{C_{bTPA}}{C_{tEG}+C_{bEG}}\right]$
Vinyl End Group Consumption	
$tEG + tVIN \xrightarrow{k_9} bEG + AA$	$R_9 = (1-x^c)\left[k_9\frac{C_{tEG}C_{tVIN}}{(1-x^c)^2}\right]$
Generation Rates[10]	
TPA	$G_{TPA} = -R_1 - R_3$
EG	$G_{EG} = -R_1 - R_2 + R_5$
W	$G_W = R_1 + R_2 + R_3 + R_4 + R_6$
tEG	$G_{tEG} = R_1 + R_2 - R_3 - R_4 - 2R_5 - 2R_6 - R_8 - R_9$
tTPA	$G_{tTPA} = R_1 - R_2 + R_3 - R_4 + R_7 + R_8$
bEG	$G_{bEG} = R_3 + R_4 + R_5 - R_7 + R_9$
bTPA	$G_{bTPA} = R_2 + R_4 - R_7 - R_8$
bDEG	$G_{bDEG} = R_6$
tVIN	$G_{tVIN} = R_7 - R_9$
AA	$G_{AA} = R_8 + R_9$

Rate Constants and Parameters[10]

reaction j	A_j	E_j	k_j
1, 2	$8.08 \times 10^{14}\ \frac{m^3}{kmol\cdot h}$	$17.6\ \frac{kcal}{mol}$	$k_j = A_j\frac{DP_R^{\,2}}{DP_n^{\,2}}\exp\left[\frac{-E_p}{RT}\right]\exp\left[\frac{-E_j}{RT}\right]$
3, 4	$4.08 \times 10^{14}\ \frac{m^3}{kmol\cdot h}$	$17.6\ \frac{kcal}{mol}$	
5, 9	$3.24 \times 10^{14}\ \frac{m^3}{kmol\cdot h}$	$18.5\ \frac{kcal}{mol}$	
6	$1.08 \times 10^{17}\ \frac{m^3}{kmol\cdot h}$	$29.8\ \frac{kcal}{mol}$	
7	$2.16 \times 10^{11}\ \frac{1}{h}$	$37.8\ \frac{kcal}{mol}$	$k_j = A_j\exp\left[\frac{-E_j}{RT}\right]$
8	$1.38 \times 10^{11}\ \frac{1}{h}$	$29.8\ \frac{kcal}{mol}$	

Table 7 (Continued)

Thermodynamic Parameters[57−59]

equilibrium reaction j	ΔS_j (cal/mol·K)	ΔH_j (cal/mol)
3, 4	−10.80	−5666
5	−19.21	−9122

Physical Properties[37]

liquid molar volume

$$\hat{\rho}_i^{\mathrm{L}}\left(\frac{\mathrm{kmol}}{\mathrm{m}^3}\right) = \frac{A_i}{B_i^{(1+(1-T/C_i)D_i)}} \text{ for } E_i \le T \le F_i$$

vapor pressure

$$P_i^{\mathrm{sat}}\ (\mathrm{Pa}) = \exp[A_i + B_i/T + C_i \ln T + D_i T^{E_i}] \text{ for } F_i \le T \le G_i$$

vapor viscosity

$$\mu_i^{\mathrm{V}}\ (\mathrm{Pa{\cdot}s}) = \frac{A_i T^{B_i}}{1 + \frac{C_i}{T} + \frac{D_i}{T^2}} \text{ for } E_i \le T \le F_i$$

Physical Property Parameters[37]

constant	ethylene glycol	water	acetaldehyde	nitrogen
		liquid molar volume (kmol/m^3)		
A_i	1.3353E+00	5.4590E+00	1.6650E+00	
B_i	2.5499E−01	3.0542E−01	2.6004E−01	
C_i	6.4500E+02	6.4713E+02	4.6100E+02	
D_i	1.7200E−01	8.1000E−02	2.7760E−01	
E_i (K)	260.15	273.16	150.15	
F_i (K)	645.00	333.15	461.00	
		vapor pressure (Pa)		
A_i	1.9464E+02	7.3649E+01	2.0607E+02	
B_i	−1.4615E+04	−7.2582E+03	−8.4786E+03	
C_i	−2.5433E+01	−7.3037E+00	−3.1548E+01	
D_i	2.0140E−05	4.1653E−06	4.6314E−02	
E_i	2.0000E+00	2.0000E+00	1.0000E+00	
F_i (K)	260.15	273.16	150.15	
G_i (K)	645.00	647.13	461.00	
		vapor viscosity (Pa·s)		
A_i	4.0788E−06	2.6986E−06	1.2220E−07	7.6320E−07
B_i	3.7031E−01	4.9800E−01	7.8700E−01	5.8823E−01
C_i	1.0567E+03	1.2577E+03	7.7000E+01	6.7750E+01
D_i	−4.0100E+04	−1.9570E+04		
E_i (K)	260.15	373.15	293.55	80.00
F_i (K)	1000.00	1073.10	1000.00	1500.00

Crystallization Kinetics[49]

degree of crystallinity

$$\frac{\mathrm{d}\phi_{\mathrm{c}}}{\mathrm{d}t} = \left[\beta_1 \exp\left(-\frac{E_x}{RT} - \frac{\psi_1 T_{\mathrm{m}}^0}{T(T_{\mathrm{m}}^0 - T)}\right) + \beta_2 \exp\left(-\frac{E_x}{RT} - \frac{\psi_2 T_{\mathrm{m}}^0}{T(T_{\mathrm{m}}^0 - T)}\right)\phi_{\mathrm{c}}\right](\phi_{\mathrm{c}}^0 - \phi_{\mathrm{c}})$$

(β_1, β_2, y_1, y_2 = constants; E_x = activation energy of the segment transfer across the nucleus-melt boundary; R = ideal-gas constant; T_{m}^0 = equilibrium melt temperature; T = absolute temperature)

constant	PET
E_x (kJ/mol)	40.24
T_{m}^0 (K)	533
Y_1 (K)	201
Y_2 (K)	201
β_1 (min^{-1})	4.33×10^6
β_2 (min^{-1})	6.6×10^4

Diffusional Mass Transfer[7,48,53,68−70]

diffusivity in polymer

$$\mathscr{D}_i^{\mathrm{P}}(T) = \mathscr{D}_{0,i}^{\mathrm{P}} \exp\left[\frac{-E_{\mathrm{D},i}}{RT}\right](1 - x_{\mathrm{c}})$$

($\mathrm{D}_i^{\mathrm{P}}$ = diffusivity within polymer; $\mathrm{D}_{0,i}^{\mathrm{P}}$ = preexponential factor; $E_{\mathrm{D},i}$ = activation energy for diffusion; R = ideal-gas constant; and T = absolute system temperature)

constant	ethylene glycol	water	acetaldehyde
$\mathrm{D}_{0,i}^{\mathrm{P}}$ (cm^2/s)	1.93E−6	0.072	0.072
$E_{\mathrm{D},i}$ (kJ/kmol)	29.670	0.03626	0.03626

diffusivity in nitrogen

$$\mathscr{D}_i^{\mathrm{V}}\left(\frac{\mathrm{cm}^2}{\mathrm{s}}\right) = \frac{0.001\,43T\ (\mathrm{K})^{1.75}}{P\ (\mathrm{bar})\sqrt{2[(1/M_i) + (1/M_j)]^{-1}}[(\sum_v)_i^{1/3} + (\sum_v)_j^{1/3}]^2} (i = \mathrm{W})$$

(T = absolute temperature; P = pressure; M_i and M_j = molecular weight; $\sum_v$ = sum of the atomic diffusion volumes; i = volatile species; j = bulk carrier gas)

Table 8. Summary of the Four Cell Model Versions for Which We Compare Simulation Results (The PDE and ODE Versions Are Used with and without Crystallization Equations)

cell model version	species balances	initial conditions	boundary conditions (i = EG, W, AA)
PDE with or without crystallization kinetics[60,63]	$V\frac{\partial C_i^{\mathrm{P}}}{\partial t} = C_{i,0}\dot{V}_0 - C_i\dot{V} + \mathscr{D}_i^{\mathrm{P}}\left[\frac{\partial^2 C_i^{\mathrm{P}}}{\partial r^2} + \frac{2}{r}\frac{\partial C_i^{\mathrm{P}}}{\partial r}\right]V + G_iV$ for (i = EG, W, AA)	$C_i^{\mathrm{P}} = C_{i,0}^{\mathrm{P}}$ for $t = 0$, $0 < r < r_{\mathrm{s}}$	center: $\frac{\mathrm{d}C_i^{\mathrm{P}}}{\mathrm{d}t} = 0$ for $t > 0$, $r = 0$ (2a)
	$V\frac{\mathrm{d}C_i^{\mathrm{P}}}{\mathrm{d}t} = C_{i,0}^{\mathrm{P}}\dot{V}_0 - C_i^{\mathrm{P}}\dot{V} + G_iV$ for ($i \neq$ EG, W, AA)		surface: $-\mathscr{D}_i^{\mathrm{P}}\left.\frac{\partial C_i^{\mathrm{P}}}{\partial r}\right\|_{r=r_{\mathrm{s}}} = k_i^{\mathrm{V}}(C_i^{\mathrm{I}} - C_i^{\mathrm{V}})$ for $t > 0$, $r = r_{\mathrm{s}}$
ODE with or without crystallization kinetics[64,65]	$V\frac{\mathrm{d}\tilde{C}_i^{\mathrm{P}}}{\mathrm{d}t} = \tilde{C}_{i,0}^{\mathrm{P}}\dot{V}_0 - \tilde{C}_i^{\mathrm{P}}\dot{V} - \frac{3k_{\mathrm{mt},i}^{\mathrm{OV}}RT(C_i^{\mathrm{I}} - C_i^{\mathrm{V}})}{r_{\mathrm{s}}}V + G_iV$ for (i = EG, W, AA)	$\tilde{C}_i^{\mathrm{P}} = \tilde{C}_{i,0}^{\mathrm{P}}$ for $t = 0$	none
	$V\frac{\mathrm{d}C_i^{\mathrm{P}}}{\mathrm{d}t} = C_{i,0}^{\mathrm{P}}\dot{V}_0 - C_i^{\mathrm{P}}\dot{V} + G_iV$ for ($i \neq$ EG, W, AA)		

group consumption. However, because of crystallinity, we make adjustments to reactant concentrations and reaction rates.

Polymer bound groups, such as bTPA and bEG, make up the crystalline phase. Other groups, such as monomer, condensates, and end groups, make up the amorphous phase. The crystalline phase, therefore, does not participate in reactions. We must calculate the amorphous concentration of monomer, condensates, and end groups in the reaction kinetics.[48]

$$C_{i,\mathrm{amorphous}} = \frac{C_{i,\mathrm{overall}}}{1 - x^{\mathrm{c}}} \tag{11}$$

We also modify the reaction rates by the amorphous fraction as in eq 12.[48]

$$R_{j,\mathrm{amorphous}} = \frac{R_{j,\mathrm{overall}}}{1 - x^{\mathrm{c}}} \tag{12}$$

To account for chain mobility, we follow the work of Kang.[10] Chain mobility is temperature-dependent as in an Arrhenius-type relationship,

$$m_{\mathrm{p}} \propto \exp\left[\frac{-E_{\mathrm{p}}}{RT}\right] \tag{13}$$

where m_{p} is the chain mobility at temperature T and E_{p} is the activation energy of translational motion. Translational mobility of polymer chains decreases with increasing length. Reptation theory[56] suggests that translational mobility is inversely proportional to the square of the chain length, quantified by the number-average degree of polymerization:

$$m_{\mathrm{p}} \propto \frac{1}{\mathrm{DP}_{\mathrm{n}}^{\,2}} \tag{14}$$

The reactions rates for esterification, polycondensation, bDEG formation, and vinyl end group consumption reactions are all proportional to the chain mobility. Thermal degradation and AA formation reactions are intramolecular, so translational motion does not affect them.

We express the equilibrium constants for the hydrolysis-esterification reactions involving bEG (reactions 3 and 4 in the Kang and co-workers[10,23,24] kinetic scheme):

$$K_{\mathrm{H,bEG}} = \exp\left[\frac{\Delta S}{R} - \frac{\Delta H}{RT}\right] \tag{15}$$

We find the polycondensation equilibrium constant (reaction 5 in the Kang and co-workers[10,23,24] kinetic scheme):

$$K_{\mathrm{C}} = \exp\left[\frac{\Delta S}{R} - \frac{\Delta H}{RT}\right] \tag{16}$$

We obtain the equilibrium constants for the hydrolysis-esterification reactions involving tEG (reactions 1 and 2 in the Kang and co-workers[10,23,24] kinetic scheme) by their relation to the other equilibrium reactions:

$$K_{\mathrm{C}} = \frac{K_{\mathrm{H,bEG}}}{K_{\mathrm{H,tEG}}} \tag{17}$$

4.6. Cell Model for Continuous Reaction and Diffusion. 4.6.1. Material Balance. We consider simultaneous reaction and diffusion in a material balance for a single cell, or CSTR. The small molecules diffuse to the surface of the pellet where the carrier stream removes them. We model diffusion in one of two ways: Fickian diffusion where mass transfer of molecules is due to a concentration gradient, and mass transfer via two-film theory using an overall convective mass-transfer coefficient. We find Fickian diffusion in the works by Devotta and Mashelkar,[14] Kang,[10] Mallon and Ray,[48] Yao and co-workers,[60,61] Kim and Jabarin,[62] and Algeri and Rovaglio,[63] while Yao et al.[64] and Rovaglio et al.[65] use the two-film theory. We will compare simulation results for models using these two approaches. Our material balance equations are in Table 8.

4.6.2. Overall Mass-Transfer Coefficient. We calculate the overall mass-transfer coefficient $k_{\mathrm{mt},i}^{\mathrm{OV}}$ as follows,

$$\frac{1}{k_{\mathrm{mt},i}^{\mathrm{OV}}\,(\mathrm{kmol/m^2{\cdot}s{\cdot}bar})} = \frac{K_i^{\mathrm{P-V}}M_i}{k_{\mathrm{mt},i}^{\mathrm{P}}\,(\mathrm{kg/m^2{\cdot}s})} + \frac{RT}{k_{\mathrm{mt},i}^{\mathrm{V}}\,(\mathrm{m/s})} \tag{18}$$

where $K_i^{\mathrm{P-V}}$ is the distribution coefficient for species i in this polymer−vapor system and $k_{\mathrm{mt},i}^{\mathrm{P}}$ is the mass-transfer coef-

ficient of species *i* in the polymer. Henry's law is a special case of the distribution coefficient for vapor−liquid systems. We relate the Henry's constant for the diffusing species *i* to its equilibrium partial pressure at the pellet surface (P_i^{I}) and its volume fraction in the polymer (ϕ_i^{P}), as in Rovaglio et al.[65] Furthermore, we use the polymer−NRTL model to calculate P_i^{I}.

$$K_i^{\mathrm{P-V}} = \frac{P_i^{\mathrm{I}}}{\phi_i^{\mathrm{P}}} \tag{19}$$

4.6.3. Mass-Transfer Coefficient in Vapor Phase. We calculate a mass-transfer coefficient[67] for volatiles in a sphere to a flowing gas,

$$k_{\mathrm{mt},i}^{\mathrm{V}}\left(\frac{\mathrm{m}}{\mathrm{s}}\right) = 1 \times 10^{-4}\frac{\mathscr{D}_i^{\mathrm{V}}\,(\mathrm{cm}^2/\mathrm{s})}{D_{\mathrm{s}}\,(\mathrm{m})}\left[2 + 0.552(N_{\mathrm{Re}})^{0.53}(N_{\mathrm{Sc}})^{1/3}\right] \tag{20}$$

where $\mathscr{D}_i^{\mathrm{V}}$ is the diffusivity of species *i* in the vapor phase, calculated with the correlation by Fuller and co-workers;[68−70] D_{s} is the diameter of a sphere of the same surface area as the pellet; N_{Re} is the dimensionless Reynolds number; and N_{Sc} is the dimensionless Schmidt number. D_{s} is not the same as the pellet diameter D_{p}, except for true spherical polymer pellets. The factor 1×10^{-4} comes from converting the diffusivity in units of cm^2/s to m^2/s.

4.6.4. Mass-Transfer Coefficient in Polymer Phase. We follow Yao et al.[64] to calculate $k_{\mathrm{mt},i}^{\mathrm{P}}$,

$$k_{\mathrm{mt},i}^{\mathrm{P}}\,(\mathrm{kg/m^2{\cdot}s}) = 1.5\,\frac{\mathscr{D}_i^{\mathrm{P}}(\mathrm{cm}^2/\mathrm{s})\rho^{\mathrm{P}}(\mathrm{kg/m}^3)\pi^2(1 \times 10^{-4})}{3r_{\mathrm{s}}} \tag{21}$$

where ρ^{P} is the density of the polymer phase. The factor 1×10^{-4} comes from converting the diffusivity in units of cm^2/s to m^2/s.

5. Simulation Results

We now simulate the entire SSP process (see Figure 1). We input the following information: (1) flow rates and compositions for fresh-feed streams; (2) conditions for unit operations; (3) initial reaction kinetic parameters; (4) initial crystallization kinetic parameters; and (5) initial diffusion coefficients. We fit all initial parameters to best match the process data.

5.1. Comparison of Model Predictions to Plant Data. We can use either Fickian diffusion or two-film theory to model diffusion. Also, we may or may not include crystallization kinetics in our model. The two options for modeling diffusion along with the option of modeling crystallization result in four possible models: (1) PDE species balance with crystallization; (2) ODE species balance with crystallization; (3) PDE species balance without crystallization; and (4) ODE species balance without crystallization. We briefly summarize the four cell models in Table 8. We then examine the predictions of each model for the important simulation targets: intrinsic viscosity, degree of crystallinity, and acetaldehyde concentration.

We construct the flowsheet in the software (Aspen Custom Modeler) sequentially from start to finish as in the actual plant: (1) precrystallizers, (2) crystallizer, (3) reactor, (4) nitrogen cooler, and (5) air cooler. The models contain 58 000 or less equations depending on its complexity for four variations of the cell model. The software stores the converged residuals of equations so it only needs to handle new residuals related to where we make changes in the process model. This reduces the computational requirements and consequently the time required to converge a new solution. It takes the software only a few seconds with an Intel Pentium 4-M 2.5 GHz CPU to determine the steady-state solution when we change the operating conditions in the process using any of the models.

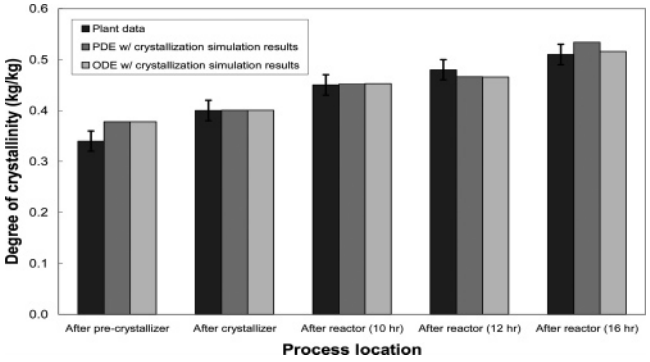

Figure 3. Number-average molecular weight simulation results and plant data throughout the process.

We predict the number-average molecular weight throughout the process for all of the cell model variations and compare them to the plant data in Figure 3. We see that we are unable to fit the data for number-average molecular weight (MWN) in the reactor using the ODE model without crystallization kinetics. However, this model performs well in describing the precrystallizer and crystallizer. The simulated MWN results from the PDE model without crystallization kinetics seem to match well with the plant data throughout the process within measurement error. We believe the results for the precrystallizer and the crystallizer match the plant data because the process is reaction-controlled rather than diffusion-controlled.

The ODE model with crystallization kinetics fits the MWN throughout the process, including the reactor. We are unable to fit the ODE model without crystallization kinetics to the data. The degree of crystallinity amplifies the polymerization rate by increasing the local concentrations of the reacting species as they are expelled from the crystallizing material. We do not see the appropriate polymerization rate increases when we neglect the increasing degree of crystallinity. Even though the reactor is diffusion-controlled, the polymerization kinetics are still important for achieving the correct MWN in the given residence time.

The PDE model without crystallization kinetics appears to fit the MWN nearly identically to the PDE model with crystallization kinetics. We must fit the diffusivity preexponential for ethylene glycol in order to get such close values for MWN. However, on deeper inspection of the PDE model without crystallization kinetics, we see that this results in a diffusivity for ethylene glycol that is much higher than that of water, which is not possible. For example, $\mathscr{D}_{\mathrm{EG}}^{\mathrm{P}}$ in the reactor for the model without crystallization kinetics ranges from 2.7×10^{-5} to 3.0×10^{-5} cm^2/s, while $\mathscr{D}_{\mathrm{W}}^{\mathrm{P}}$ ranges from 7.5×10^{-6} to 7.9×10^{-6} cm^2/s. Therefore, the results of the model without crystallization kinetics, which happen to fall within measurement error of the data, are invalid.

Note that we simulate the entire process and *not* individual unit operations. This has several implications. For example, if a particular model such as the ODE with no crystallization gives poor predictions for acetaldehyde concentration, these poor predictions are fed as inputs to the crystallizer model. Any prediction error inherent in the crystallizer model is superim-

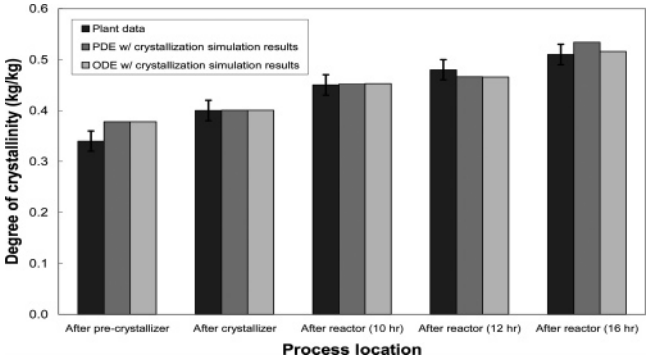

Figure 4. Simulation results and plant data for degree of crystallinity throughout the process.

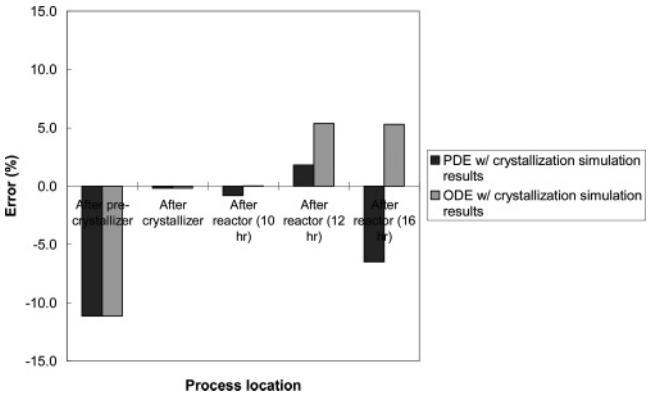

Figure 5. Error percentages for degree of crystallinity results.

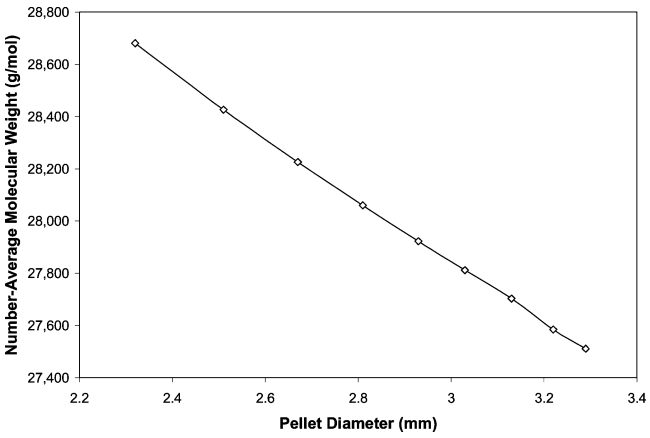

Figure 6. Simulation results showing the effect of varying pellet length on number-average molecular weight.

posed over the prediction error of the precrystallizer. Therefore, our validation studies cannot tell us which theoretical model (ODE vs PDE, crystallization kinetics vs no crystallization kinetics) is best to model a particular unit operation; rather, our validation studies only suggest which option is best *for modeling the entire SSP process*. The inability of a particular model to fit the plant data only suggests that we are unable to easily find a set of reaction/diffusion parameters to fit the data. It does not suggest that a particular model cannot fit the data with any parameter set. To illustrate this point further, we consider another example. Crystallinity sometimes changes little within the SSP reactor—however, since we are modeling precrystallizers and crystallizers in addition to the SSP reactor, we should include crystallization in all models. For those practitioners who wish to model only the SSP reactor, it may be allowable to neglect crystallization rate considerations.

Table 9. C_{AA} Predictions from the Four Cell Models (Plant Data for the Concentration After 10 h in the Reactor is 2 ppm)

cell model version	C_{AA} after reactor (10 h) (ppm)
PDE with crystallization kinetics	2.0
ODE with crystallization kinetics	1E−6
PDE without crystallization kinetics	2.0
ODE without crystallization kinetics	1E−6

Table 10. Final Diffusivity Parameters for Volatiles in Polymer Used in the Model

component i	$D^{p}_{i,0}$ (cm^2/s)	E_D,i (kJ/kmol)
W	2.3E−4	10048
EG	4.9E−5	16747
AA	8.9E−6	10048

We now focus only on the cell models that include crystallization kinetics when we predict the degree of crystallinity. We present the results in Figure 4 and the corresponding error percentages relative to the plant data in Figure 5.

Both the PDE and ODE models predict degree of crystallinity well for the most part, but there is a problem in the precrystallizer. Moisture in the air may affect the crystallization rate, but the crystallization kinetics that we use do not account for this. The errors for the different reactor residence times are a direct result of the intrinsic viscosity prediction errors. The degree of crystallinity in the reactor changes from control by the crystallization kinetics to control by the molecular weight.

Moving on to acetaldehyde predictions, we know that C_{AA} after a reactor residence time of 10 h is 2 ppm or less, while the feed concentration is 11 ppm. Table 9 compares the predicted final C_{AA} from the four cell models. We are unable to identify a suitable parameter set to make the ODE models accurately predict acetaldehyde concentration. However, we are able to easily determine a suitable parameter set for the PDE models.

Table 10 lists our mass-transfer parameters for the PDE model with crystallization kinetics. We use the diffusivity activation energies for water and ethylene glycol from Kang.[10] We assume acetaldehyde has the same activation energy as water. We fit diffusivity preexponential factors for all volatiles to match acetaldehyde concentration and intrinsic viscosity.

5.2. Sensitivity Studies. We investigate, using our PDE cell model with crystallization kinetics, the following two sensitivities: (1) the effect of varying the pellet length and (2) the effect of varying the reactor temperature profile.

We set the reactor residence time at 12 h and vary the length of the pellet. We wish to see how the number-average molecular weight (MWN) varies with the pellet length. The cross-sectional area of the pellets is 3.2 mm × 3.2 mm. The length is 2.5 mm. We choose pellet lengths from 1.5 to 3.5 mm. We see in Figure 6 that our model predicts that MWN is relatively insensitive to pellet length for this range of pellet lengths.

We now increase the reactor temperature up by 12 °C. We wish to see the effect that the temperature profile has on the product. Figure 7 shows that our model prediction for MWN depends on temperature.

5.3. Dynamic Response. We are able to show that our cell model gives steady-state simulation results that can match the plant data within measurement error. We need to check the applicability of the cell model for a dynamic simulation, where axial dispersion can have a significant impact on the dynamic response.

Each cell assumes perfect mixing and, therefore, will have more or less axial dispersion depending on the number of cells

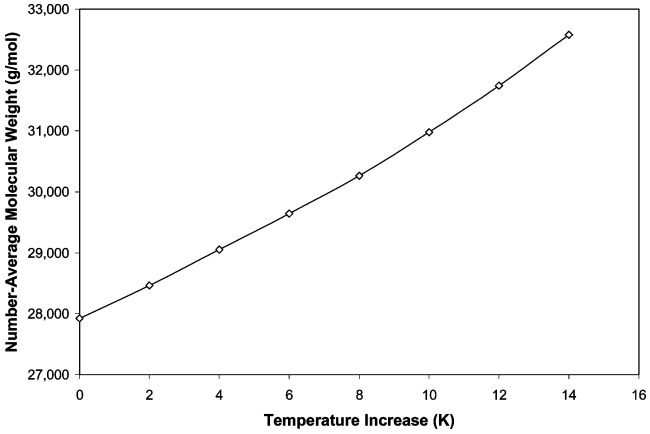

Figure 7. Raising the reactor temperature profile increases the final number-average molecular weight. Results are for a reactor residence time of 12 h.

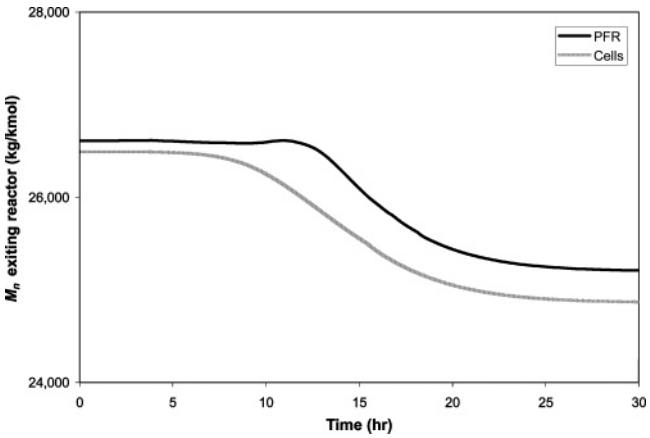

Figure 8. Dynamic response in M_n exiting the reactor after a step change to a lower-grade prepolymer chip feed.

chosen to model a particular unit operation. An ideal plug-flow reactor (PFR) has zero axial dispersion. We would need a very large number of cells to model a PFR with zero axial dispersion. We can compare the dynamic response of our cell model and the PFR model for the SSP reactor. We perform a step change with the prepolymer pellet feed in which we change from a 0.65 dL/g grade to a lower, 0.63 dL/g grade chip. We maintain all operating conditions and model the preceding precrystallizers and crystallizer with cell models. Figure 8 shows the dynamic change in M_n for the chip exiting the reactor. Note that the steady-state values of M_n in the cell model (with 8−12 cells) compare favorably to those in the PFR model.

We see that it takes several hours for the M_n in the PFR model to start dropping versus that in the cell model. The axial dispersion in all of the cell models (precrystallizers, crystallizer, and reactor) causes a long, smooth transition to the final M_n. The M_n change in the PFR model is sharper, but it does not look like a clear step change because of the axial dispersion in the precrystallizers and the crystallizer. Still, the response in the PFR is more along the lines of what we expect versus that in the cell models. We can conclude that the cell models perform worse than the PFR models in dynamic simulations unless we use a much higher number of cells to limit axial dispersion.

6. Model Application: New Product Design

Industry uses solid-state PET resin in textile fiber, bottles for carbonated beverages, trays for frozen foods that are safe for use in microwave and convection ovens, and tire cord.[17,21] These applications require different intrinsic viscosities. Duh[17,27] offers typical intrinsic viscosity ranges for numerous applications: 0.57−0.65 dL/g for textile-fiber-grade resins; 0.72−0.85 dL/g for bottle-grade resins; 0.85−0.95 dL/g for tray resins; and 0.95−1.05 dL/g for tire-cord resins.

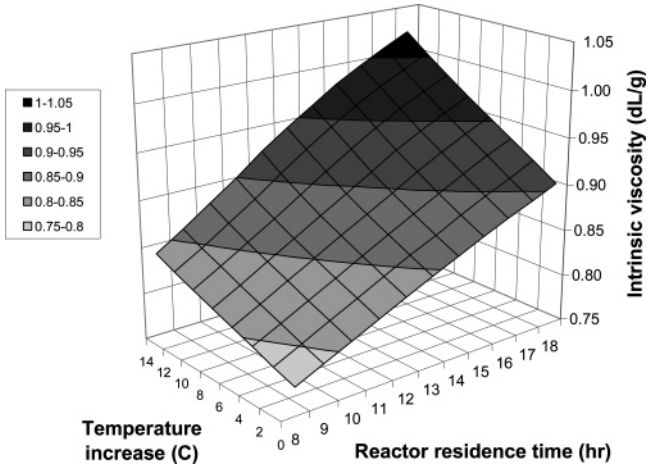

Figure 9. Intrinsic viscosity predictions for a variety of reactor residence times and temperatures. Intrinsic viscosity results correspond to measurements at 25 °C in phenol/tetrachloroethane (3:2).

Conventional melt polymerization processes yield a prepolymer with a $[\eta]$ of ∼0.35−0.60 dL/g.[20] Conventional SSP processes raise the $[\eta]$ to ∼1.0 dL/g.[21] The plant's PET SSP process currently produces solid-state PET with a $[\eta]$ from 0.81 to 0.87 dL/g. We now use our model to determine the operating conditions necessary to raise the $[\eta]$ further from 0.87 to 1.0 dL/g.

There are several ways to attain the maximum intrinsic viscosity for a given prepolymer, including the following: (1) optimize pellet size; (2) optimize inert gas velocity in the reactor; (3) optimize reactor temperature; (4) optimize polymerization time (reactor residence time); (5) optimize prepolymer $[\eta]$; (6) optimize prepolymer crystallinity; and (7) optimize catalyst concentration. Our prepolymer pellets do not contain any added catalyst, so we do not consider any changes in catalyst concentration.

We maintain the pellet size (3.2 mm × 3.2 mm × 2.5 mm), carrier gas velocities, prepolymer intrinsic viscosity, prepolymer crystallinity, and zero catalyst concentration. We look for the combinations of polymerization time and reactor temperature to produce a 1.0 dL/g product.

We simulate the entire process with a 0−14 °C temperature increases for 8−18 h residence times in the SSP reactor. We plot the results in Figure 9 and look for conditions which produce the desired polymer grade.

We see that only a small set of conditions within the allowable ranges of temperature and time can meet or exceed the desired 1.0 dL/g. We must use a higher temperature and residence time.

The sticking temperature of partially crystalline PET is ∼230 °C. The optimum temperature for SSP is between 5 and 20 °C below this temperature.[21] The temperature profile with a 12 °C increase is partially within the ideal range. Pellet agglomeration should, therefore, not be a problem.

7. Conclusions

We have successfully modeled the entire poly(ethylene terephthalate) (PET) solid-state polymerization (SSP) process using a unified cell-model approach. This approach builds complex unit-operation models using individual cells, or continuous-stirred-tank reactor (CSTR) models. We combine

the cells in either parallel or series to approximate the mixing behavior of precrystallizers, crystallizers, SSP reactors, and dryers. Each cell model simultaneously accounts for reaction and diffusion. These are the fundamental mechanisms that occur throughout the entire SSP process.

We consider two models for diffusion: a partial differential equation that explicitly tracks diffusing-component concentration throughout the pellet radius and the simpler two-film theory. The two-film theory representation of mass transfer is easier to use; however, we are unable to identify suitable parameters to match our plant data. We also consider whether or not we need to model crystallization. Since we are modeling the entire SSP process, which contains precrystallizers and crystallizers, we find that we most likely should model crystallization and its effect on diffusion and reaction.

After validating our SSP model, we apply it to study the sensitivity of our SSP process on temperature and pellet geometry. For pellets with cross-sectional dimensions of 3.2 mm × 3.2 mm, we vary the length from 1.5 to 3.5 mm and predict intrinsic viscosity. The model suggests only a mild dependence of intrinsic viscosity on pellet length. In contrast, temperature changes in the SSP reactor significantly affect final intrinsic viscosity. Our model suggests that, for an increase in temperature of 12 °C, intrinsic viscosity rises by almost 0.1 dL/g. We then predict that, to produce a high-viscosity product (1 dL/g), we should simultaneously increase the reactor temperature as well as increase the residence time.

Acknowledgment

We thank Alliant Techsystems (particularly Ken Dolph, Vice President), Aspen Technology (particularly Zhiming Huang, General Manager for Greater China; Vikas Dhole, Director of Worldwide University Programs; Chau-Chyun Chen, Senior Technology Fellow; Mark E. Fusco, President; and Larry Evans, Founder), China Petroleum and Chemical Corporation (particularly Xianghong Cao, Chief Technical Officer; and Tianpu Wang, President), Formosa Petrochemical Corporation (particularly Wilfred Wang, President), Milliken Chemical (particularly John Rakers, President; and Ed Zhao, Director of Research and Development), and Honeywell Specialty Materials and Honeywell International Foundation for supporting our educational programs in computer-aided design and process systems engineering at Virginia Tech.

Nomenclature

English Symbols

a = cross-sectional area, m^2
A_j = frequency factor for reaction j, m^3/kmol/hr ($j = 1-6, 9$), 1/hr ($j = 7, 8$)
$C_{i_p}^{I}$ = interfacial concentration of species i, kg/m^3
C_i^P = concentration of species i in the polymer, kg/m^3
$C_{i,0}^P$ = initial concentration of species i in the polymer, kg/m^3
C_i^V = concentration of species i in the vapor phase, kg/m^3
$\mathscr{D}_i^P$ = diffusivity of species i in polymer, cm^2/s
$\mathscr{D}_i^V$ = diffusivity of species i in vapor, cm^2/s
$\mathscr{D}_{i,0}^P$ = preexponential factor for diffusivity of species i, cm^2/s
D_p = pellet diameter that maintains S_p/V_p, m
D_s = diameter of same surface area as the pellet, m
DP_n = number-average degree of polymerization
DP_R = reference number-average degree of polymerization
$E_{D,i}$ = activation energy of diffusion, kJ/kmol
E_j = activation energy of reaction j, kcal/mol
E_p = activation energy of translational motion, kcal/mol
E_x = activation energy of transfer of a segment through the nucleus-melt interface, kJ/mol
F_i = fraction of segment i
G_i = generation rate for species i, kmol/m^3/hr
H_j = enthalpy of reaction j, cal/mol
$k_{mt,i}^{OV}$ = overall mass-transfer coefficient of species i, kmol/m^2/s/bar
$k_{mt,i}^{P}$ = mass-transfer coefficient of species i in the polymer, kg/m^2/s
$k_{mt,i}^{V}$ = mass-transfer coefficient of species i in the vapor phase, m/s
k_j = forward rate constant for reaction j, m^3/kmol/hr
k_j' = reverse rate constant for reaction j, m^3/kmol/hr
K_j = equilibrium constant for reaction j
$\dot{m}^V$ = mass flow rate of vapor phase, kg/hr
M_i = molecular weight of segment i, kg/kmol
M_n = number-average molecular weight, kg/kmol
M_{seg} = average molecular weight of segments, kg/kmol
M_v = viscosity-average molecular weight, kg/kmol
M_w = weight-average molecular weight, kg/kmol
N_i = number of moles of species i, kmol
N_{Re} = Reynolds number
N_{Sc} = Schmidt number
P = pressure, bar
P_i^I = equilibrium partial pressure at the pellet surface, bar
P_i^{sat} = vapor pressure of species i, bar
r = radial domain, m
r_s = radius of sphere, m
R = ideal gas constant
R_j = reaction rate for reaction j, kmol/m^3/hr
S_j = entropy of reaction j, cal/mol/K
S_p = pellet surface area, m^2
t = time, hr
T = temperature, K
T_g = glass-transition temperature, K
T_m = melting-point temperature, K
T_m^0 = equilibrium melting-point temperature, K
V = system volume, m^3
$\dot{V}$ = volumetric flow rate, m^3/hr
$\dot{V}_0$ = volumetric flow rate, m^3/hr
V_p = pellet volume, m^3
V_s = volume of sphere, m^3
x^a = amorphous mass fraction, kg/kg
x^c = crystalline mass fraction, kg/kg

Greek Symbols

β_1, β_2 = crystallization kinetics parameter, min^{-1}
γ_i = activity coefficient of species i
ϵ = voidage
$[\eta]$ = intrinsic viscosity, dL/g
λ_i = ith moment for polymer chains
ρ^a = amorphous phase density, kg/m^3
ρ^c = crystalline phase density, kg/m^3
ρ^V = vapor-phase density, kg/m^3
ρ_{lim} = limiting density, kg/m^3
μ^V = vapor-phase viscosity, cP
τ = residence time, hr
ψ_1, ψ_2 = crystallization kinetics parameter, K
ϕ^c = degree of crystallinity (volume basis), m^3/m^3

$\phi^{c,0}$ = equilibrium degree of crystallinity (volume basis), m^3/m^3
Φ_s = sphericity

Literature Cited

(1) Khare, N. P.; Seavey, K. C.; Liu, Y. A.; Ramanathan, S.; Lingard, S.; Chen, C.-C. Steady-State and Dynamic Modeling of Commercial Slurry High-Density Polyethylene (HDPE) Processes. *Ind. Eng. Chem. Res.* **2002**, *41*, 5601.

(2) Seavey, K. C.; Liu, Y. A.; Lucas, B.; Khare, N. P.; Lee, T.; Pettrey, J.; Williams, T. N.; Mattson, J.; Schoenborn, E.; Larkin, C.; Hu, H.; Chen, C.-C. New Mass-Transfer Model for Simulating Industrial Nylon-6 Production Trains. *Ind. Eng. Chem. Res.* **2004**, *43*, 5063.

(3) Khare, N. P.; Lucas, B.; Seavey, K. C.; Liu, Y. A.; Sirohi, A.; Ramanathan, S.; Lingard, S.; Song, Y.; Chen, C.-C. Steady-State and Dynamic Modeling of Gas-Phase Polypropylene Processes Using Stirred-Bed Reactors. *Ind. Eng. Chem. Res.* **2004**, *43*, 884.

(4) Gostoli, C.; Pilati, F.; Sarti, G. C.; Di Giacomo, B. Chemical Kinetics and Diffusion in Poly(butylenes terephthalate) Solid-State Polycondensation: Experiments and Theory. *J. Appl. Polym. Sci.* **1984**, *29*, 2873.

(5) Chen, S.-A.; Chen, F.-L. Kinetics of Polyesterification III: Solid-State Polymerization of Polyethylene Terephthalate. *J. Polym. Sci., Part A: Polym. Chem.* **1987**, *25*, 533.

(6) Kaushik, A.; Gupta, S. K. A Molecular Model for Solid-State Polymerization of Nylon 6. *J. Appl. Polym. Sci.* **1992**, *45*, 507.

(7) Yoon, K. H.; Kwon, M. H.; Jeon, M. H.; Park, O. O. Diffusion of Ethylene Glycol in Solid State Poly(ethylene terephthalate). *Polym. J.* **1993**, *25*, 219.

(8) Kulkarni, M. R.; Gupta, S. K. Molecular Model for Solid-State Polymerization of Nylon 6. II. An Improved Model. *J. Appl. Polym. Sci.* **1994**, *53*, 85.

(9) Wu, D.; Chen, F.; Li, R.; Shi, Y. Reaction Kinetics and Simulations for Solid-State Polymerization of Poly(ethylene terephthalate). *Macromolecules* **1997**, *30*, 6737.

(10) Kang, C.-K. Modeling of Solid-State Polymerization of Poly-(ethylene terephthalate). *J. Appl. Polym. Sci.* **1998**, *68*, 837.

(11) Li, L.; Huang, N.-X.; Liu, Z.-H.; Tang, Z.-L.; Yung, W.-S. Simulation of Solid-State Polycondensation of Nylon-66. *Polym. Adv. Technol.* **2000**, *11*, 242.

(12) Wang, X.-Q.; Deng, D.-C. A Comprehensive Model for Solid-State Polycondensation of Poly(ethylene terephthalate): Combining Kinetics with Crystallization and Diffusion of Acetaldehyde. *J. Appl. Polym. Sci.* **2002**, *83*, 3133.

(13) Hsu, L.-C. Synthesis of Ultrahigh Molecular Weight Poly(ethylene terephthalate). *J. Macromol. Sci. Phys.* **1967**, *B1*, 801.

(14) Devotta, I.; Mashelkar, R. A. Modelling of Polyethylene Terephthalate Reactors—X. A Comprehensive Model for Solid-State Polycondensation Process. *Chem. Eng. Sci.* **1993**, *48*, 1859.

(15) Tang, Z.-L.; Gao, Q.; Huang, N.-X.; Sironi, C. Solid-State Polycondensation of Poly(ethylene terephthalate): Kinetics and Mechanism. *J. Appl. Polym. Sci.* **1995**, *57*, 473.

(16) Gao, Q.; Huang, N.-X.; Tang, Z.-L.; Gerking, L. Modelling of Solid State Polycondensation of Poly(ethylene terephthalate). *Chem. Eng. Sci.* **1997**, *52*, 371.

(17) Duh, B. Reaction Kinetics for Solid-State Polymerization of Poly-(ethylene terephthalate). *J. Appl. Polym. Sci.* **2001**, *81*, 1748.

(18) Xie, J.-J. Kinetics of the Solid-State Polymerization of Nylon-6. *J. Appl. Polym. Sci.* **2002**, *84*, 616.

(19) Balint, L. J.; Abos, R. L.; Snider, O. E. Process for crystallization, drying and solid-state polymerization of polyesters. U.S. Patent 3,544,525, 1970.

(20) Brent, J. W.; Shelley, L. E. Preparation of high molecular weight polyester. U.S. Patent 4,254,253, 1981.

(21) Cohn, G. Preparation of ultra-high molecular weight polyester. U.S. Patent 4,792,573, 1988.

(22) Van Krevelen, D. W. *Properties of Polymers: Their Correlation with Chemical Structure; Their Numerical Estimation and Prediction from Additive Group Contributions*, 3rd ed.; Elsevier: New York, 1990.

(23) Kang, C.-K.; Lee, B. C.; Ihm, D. W. Modeling of Semibatch Direct Esterification Reactor for Poly(ethylene terephthalate) Synthesis. *J. Appl. Polym. Sci.* **1996**, *60*, 2007.

(24) Kang, C.-K.; Lee, B. C.; Ihm, D. W.; Tremblay, D. A. A Simulation Study on Continuous Direct Esterification Process for Poly(ethylene terephthalate) Synthesis. *J. Appl. Polym. Sci.* **1997**, *63*, 163.

(25) Besnoin, J.-M.; Choi, K. Y. Identification and Characterization of Reaction Byproducts in the Polymerization of Polyethylene Terephthalate. *J. Macromol. Sci., Rev. Macromol. Chem. Phys.* **1989**, *C29*, 55.

(26) Jabarin, S. A.; Lofgren, E. A. Solid State Polymerization of Poly-(ethylene Terephthalate): Kinetic and Property Parameters. *J. Appl. Polym. Sci.* **1986**, *32*, 5315.

(27) Duh, B. Effects of the Carboxyl Concentration on the Solid-Sate Polymerization of Poly(ethylene terephthalate). *J. Appl. Polym. Sci.* **2002**, *83*, 1288.

(28) Zimmerman, J. Equilibria in Solid Phase Polyamidation. *J. Polym. Sci., Polym. Lett. Ed.* **1964**, *2*, 955.

(29) Bokis, C. P.; Orbey, H.; Chen, C.-C. Properly Model Polymer Processes. *Chem. Eng. Prog.* **1999**, *95* (4), 39.

(30) Renon, H.; Prausnitz, J. M. Local Compositions in Thermodynamic Excess Functions for Liquid Mixtures. *AIChE J.* **1968**, *14*, 135.

(31) Renon, H.; Prausnitz, J. M. Estimation of Parameters for the NRTL Equation for Excess Gibbs Energies of Strongly Nonideal Liquid Mixtures. *Ind. Eng. Chem. Process Des. Dev.* **1969**, *8*, 413.

(32) Chen, C.-C. A Segment-Based Local Composition Model for the Gibbs Energy of Polymer Solutions. *Fluid Phase Equilib.* **1993**, *83*, 301.

(33) Huggins, M. L. Solutions of Long Chain Compounds. *J. Chem. Phys.* **1941**, *9*, 440.

(34) Flory, P. J. Thermodynamics of High Polymer Solutions. *J. Chem. Phys.* **1941**, *9*, 660.

(35) Yamada, T.; Imamura, Y.; Makimura, O. A Mathematical Model for Computer Simulation of a Direct Continuous Esterification Process between Terephthalic Acid and Ethylene Glycol: Part 1. Model Development. *Polym. Eng. Sci.* **1985**, *25*, 788.

(36) Seavey, K. C.; Khare, N. P.; Liu, Y. A.; Williams, T. N.; Chen, C.-C. A New Phase-Equilibrium Model for Simulating Industrial Nylon-6 Production Trains. *Ind. Eng. Chem. Res.* **2003**, *42*, 3900.

(37) Daubert, T. E.; Danner, R. P. *Physical and Thermodynamic Properties of Pure Chemicals: Data Compilation*; Hemisphere Publishing Corporation: New York, 1989.

(38) Koepp, H. M.; Wemer, H. Endgruppenbestimmug und molekulare Verteilung bei Polyäthylenterephthalat. *Makromol. Chem.* **1959**, *32*, 79.

(39) Stevens, M. P. *Polymer Chemistry: An Introduction*, 3rd ed.; Oxford University Press: New York, 1999.

(40) Flory, P. J. *Principles of Polymer Chemistry*; Cornell University Press: Ithaca, NY, 1953.

(41) Rule, M. Physical Constants of Poly(oxyethylene-oxyterephthaloyl) (Poly(ethylene terephthalate)). In *Polymer Handbook*, 4th ed.; Brandrup, J., Immergut, E. H., Grulke, E. A., Eds.; Wiley-Interscience: New York, 1999.

(42) Berkowitz, S. Viscosity-Molecular Weight Relationships for Poly-(ethylene Terephthalate) in Hexafluoroisopropanol-Pentafluorophenol Using SEC-LALLS. *J. Appl. Polym. Sci.* **1984**, *29*, 4353.

(43) Schultz, J. M. *Polymer Crystallization: The Development of Crystalline Order in Thermoplastic Polymers*; Oxford University Press: New York, 2001.

(44) Avrami, M. Kinetics of Phase Change. I. General Theory. *J. Chem. Phys.* **1939**, *7*, 1103.

(45) Avrami, M. Kinetics of Phase Change. II. Transformation-Time Relations for Random Distribution of Nuclei. *J. Chem. Phys.* **1940**, *8*, 212.

(46) Avrami, M. Kinetics of Phase Change. III. Granulation, Phase Change and Microstructure. *J. Chem. Phys.* **1941**, *9*, 177.

(47) Malkin, A. Ya.; Beghishev, V. P.; Keapin, I. A.; Bolgov, S. A. General Treatment of Polymer Crystallization Kinetics—Part 1. A New Macrokinetic Equation and its Experimental Verification. *Polym. Eng. Sci.* **1984**, *24*, 1396.

(48) Mallon, F. K.; Ray, W. H. Modeling of Solid-State Polycondensation. I. Particle Models. *J. Appl. Polym. Sci.* **1998**, *69*, 1233.

(49) Malkin, A. Ya.; Beghishev, V. P.; Keapin, I. A. Macrokinetics of Polymer Crystallization. *Polymer* **1983**, *24*, 81.

(50) Cobbs, W. H., Jr.; Burton, R. L. Crystallization of Polyethylene Terephthalate. *J. Polym. Sci.* **1953**, *X*, 275.

(51) Chang, T. M. Kinetics of Thermally Induced Solid State Polycondensation of Poly(Ethylene Terephthalate). *Polym. Eng. Sci.* **1970**, *10*, 364.

(52) Whitehead, B. D. The Crystallization and Drying of Polyethylene Terephthalate (PET). *Ind. Eng. Chem. Process Des. Dev.* **1977**, *16*, 341.

(53) Schmalz, E. O.; Grundke, H. Water Diffusion into High Polymers. *Faserforsch. Textiltech.* **1969**, *20*, 377.

(54) Ravindranath, K.; Mashelkar, R. A. Modeling of Poly(ethylene Terephthalate) Reactors. I. A Semibatch Ester Interchange Reactor. *J. Appl. Polym. Sci.* **1981**, *26*, 3179.

(55) Gaymans, R. J; Amirtharaj, J; Kamp, H. Nylon 6 Polymerization in the Solid State. *J. Appl. Polym. Sci.* **1982**, *27*, 2513.

(56) de Gennes, P.-G. *Scaling Concepts in Polymer Physics*; Cornell University Press: Ithaca, NY, 1979; p 227.

(57) Reimschuessel, H. K.; Debona, B. T.; Murthy, A. K. S. Kinetics and Mechanism of the Formation of Glycol Esters: Benzoic Acid—Ethylene Glycol System. *J. Polym. Sci., Polym. Chem. Ed.* **1979**, *17*, 3217.

(58) Reimschuessel, H. K.; Debona, B. T. Terephthalic Acid Esterification Kinetics: 2-(2-Methoxyethoxy)ethyl Terephthalates. *J. Polym. Sci., Polym. Chem. Ed.* **1979**, *17*, 3241.

(59) Reimschuessel, H. K. Poly(ethylene terephthalate) Formation. Mechanistic and Kinetic Aspects of the Direct Esterification Process. *Ind. Eng. Chem. Prod. Res. Dev.* **1980**, *19*, 117.

(60) Yao, K. Z.; McAuley, K. B.; Berg, D.; Marchildon, E. K. A Dynamic Mathematical Model for Continuous Solid-Phase Polymerization of Nylon 6,6. *Chem. Eng. Sci.* **2001**, *56*, 4801.

(61) Yao, K. Z.; McAuley, K. B. Simulation of Continuous Solid-Phase Polymerization of Nylon 6,6 (II): Processes with Moving Bed Level and Changing Particle Properties. *Chem. Eng. Sci.* **2001**, *56*, 5327.

(62) Kim, T. Y.; Jabarin, S. A. Solid-State Polymerization of Poly(ethylene terephthalate). II. Modeling Study of the Reaction Kinetics and Properties. *J. Appl. Polym. Sci.* **2003**, *89*, 213.

(63) Algeri, C.; Rovaglio, M. Dynamic Modeling of a Poly(ethylene terephthalate) Solid-State Polymerization Reactor I: Detailed Model Development. *Ind. Eng. Chem. Res.* **2004**, *43*, 4253.

(64) Yao, K. Z.; McAuley, K. B.; Marchildon, E. K. Simulation of Continuous Solid-Phase Polymerization of Nylon 6,6. III. Simplified Model. *J. Appl. Polym. Sci.* **2003**, *89*, 3701.

(65) Rovaglio, M.; Algeri, C.; Manca, D. Dynamic Modeling of a Poly(ethylene terephthalate) Solid-State Polymerization Reactor II: Model Predictive Control. *Ind. Eng. Chem. Res.* **2004**, *43*, 4267.

(66) Ravindranath, K.; Mashelkar, R. A. Polyethylene Terephthalate—I. Chemistry, Thermodynamics and Transport Properties. *Chem. Eng. Sci.* **1986**, *41*, 2197.

(67) Geankoplis, C. J. *Transport Processes and Unit Operations*, 3rd ed.; Prentice Hall PTR: Upper Saddle River, NJ, 1993.

(68) Fuller, E. N.; Giddings, J. C. A Comparison of Methods for Predicting Gaseous Diffusion Coefficients. *J. Gas Chromatogr.* **1965**, *3*, 222.

(69) Fuller, E. N.; Schettler, P. D.; Giddings, J. C. A New Method for Prediction of Binary Gas-Phase Diffusion Coefficients. *Ind. Eng. Chem.* **1966**, *58*, 18.

(70) Fuller, E. N.; Ensley, K.; Giddings, J. C. Diffusion of Halogenated Hydrocarbons in Helium. The Effect of Structure on Collision Cross Sections. *J. Phys. Chem.* **1969**, *73*, 3679.

Received for review February 16, 2006
Revised manuscript received August 5, 2006
Accepted October 10, 2006

IE0601955